CONEM 2016
CONGRESSO NACIONAL DE ENGENHARIA MECÂNICA
21 - 25 AGOSTO DE 2016
FORTALEZA - CEARÁ

CORROSION BEHAVIOR OF LOW-TEMPERATURE PLASMA CARBURIZED AISI 420 STEEL - PART II - EFFECT OF TREATMENT TIME

Cristiano José Scheuer, cristiano.scheuer@gmail.com[1,2]
Rodrigo Perito Cardoso, rodrigo.perito@ufpr.br[1]
Felipe Possoli, felipepossoli@gmail.com[3]
Paulo César Borges, pborges@utfpr.edu.br[3]
Silvio Francisco Brunatto, brunatto@ufpr.br[1]

[1] Plasma Assisted Manufacturing Technology & Powder Metallurgy Group, UFPR, 80531-980, Curitiba, PR, Brazil.
[2] Industrial Technical College, UFSM, 97105-900, Santa Maria, RS, Brazil.
[3] Academic Department of Mechanic, UTFPR, 80230-901, Curitiba, PR, Brazil.

Abstract: *The effect of plasma treatment parameters on the corrosion behavior of low-temperature carburized AISI 420 stainless steel was investigated by means of electrochemical measurements. The second part of this study (out of two), was conducted in order to evaluate the effect of the treatment time on carburized samples corrosion resistance. Plasma carburizing treatments were performed at 400°C (for times from 12 to 48 h) and 450°C (for times from 4 to 16 h). The corrosion behavior was evaluated through open circuit potential and cyclic polarization test, using a solution of 3.0% NaCl as electrolyte. To support the discussions on corrosion behavior, XRD, microstructural analysis, and hardness measurements were also carried out. The results showed that corrosion potential decreased with treatment times increased on the range of 12 to 48 h for treatments performed at 400 °C. For treatments realized at 450 °C corrosion potential increases from 4 to 8 h and decreasing subsequently for 12 and 16 h to. Furthermore, It was also found that long-term treatment (16 h for 450 °C and 48 h for 400 °C) showed smaller corrosion potential that the untreated sample. Finally, an analysis of the corroded surface showed the predominance of pitting corrosion mechanism on carburized samples, and widespread corrosion to the untreated sample.*

Palavras-chave: *low-temperature plasma carburizing, treatment parameters, martensitic stainless steel, expanded martensite, corrosion resistance, electrochemical tests.*

1. INTRODUCTION

Martensitic stainless steels (MSS) are largely employed on applications where mechanical properties are the primary requirement (Li and Bell, 2006; Li and Bell, 2007). However, these steels find limited applications where a high corrosion resistance is required in addition to mechanical properties (Lu *et al.* 2015). In order to overcome this limitation, several authors have been dedicated to the optimization of the MSS electrochemical properties using surface engineering techniques. Among the treatments available for this purpose, the application of plasma assisted thermochemical treatments have result in a beneficial effect on corrosion resistance of martensitic stainless steels, as shown by Li and Bell (2006), Li and Bell (2007), Xi *et al.* (2008[a,b,c]), Corengia *et al*. (2004), Corengia *et al*. (2006), Souza *et al.* 2008, Figueroa *et al*. (2005), Kim *et al.* (2003), Alphonsa *et al.* (2002), and Sun *et al.* (1994).

In contrast to very intensive research and development activities on corrosion behavior of plasma nitrided MSS, much less attention has been given to the effect of plasma carburizing application on this feature. In specialized literature, it is only found the work published by Li and Bell (2007), where non-promising results are presented (with respect to mechanical, tribological and electrochemical properties). In contrast, it was demonstrated by Scheuer *et al.* (2012[a,b]), Scheuer *et al.* (2013) and Scheuer *et al.* (2016), that with a adequate choice of electrical discharge and treatment parameters, promising results can be achieved by low-temperature plasma carburizing application on MSS.

Selection of appropriate carburizing parameters appears as an important issue when ensuring optimal performance characteristics of the MSS. Inadequate choice of the stainless steels processing conditions can lead to precipitation of chromium-rich carbides in the grain boundaries vicinity and martensitic laths (Frangini and Mignone, 1992; Aydoğdu and Aydinol, 2006; Alonso-Falleiros *et al.* 1999; Kain *et al.* 2005, Aquino *et al.* 2009; Tavaresi et al. 2010). Thus, chromium depleted zones are formed adjacent to the precipitated carbides causing the sensitization

(Taji *et al.* 2005). As a result, the chromium-depleted region of the carburized layer cannot form a protective passive film.

Considering the published papers that demonstrate the possibilities of optimizing the corrosion resistance of MSS by low-temperature plasma nitriding (Li and Bell, 2006; Li and Bell, 2007; Xi *et al.* 2008[a,b,c]; Corengia *et al*. 2004; Figueroa *et al*. 2005; Bernardelli *et al.* 2010; Brühl *et al.* 2010), and considering that the determining of minimum process time condition is an important economic factor, the aiming of this work is evaluating the influence of treatment and time on the corrosion resistance of carburized AISI 420 steel.

2. EXPERIMENTAL PROCEDURE

2.1 Samples preparation

Cylindrical samples of 10 mm in height and 50.8 mm in diameter were cut from AISI 420 steel commercial rod (composition obtained by X-ray fluorescence: 0.31% C, 0.75% Mn, 0.36% Si, 13.68% Cr, 0.17%Ni, 0.04% P, 0.03% S, 0.06%Cu and Fe balance, in wt.%), supplied in the annealed condition, presenting a gross-equiaxed ferrite grain matrix and chromium carbide precipitates. To obtain a *bct* martensite structure, samples were air quenched from 1050 °C, after 0.5 h at the austenitizing temperature (the sample hardness in the as-quenched condition was 576±12 $HV_{0.3}$). After heat treatment, samples were ground using SiC sandpaper ranging from 100 to 1200 grade and polished using 1 μm Al_2O_3 abrasive suspension, in order to obtain a final mirror finish of a mean roughness Ra value around than 0.07 μm. Finally, samples were alcohol cleaned in ultrasonic bath and then introduced into the discharge chamber. Tempering and carburizing were simultaneously carried out. For comparison purpose, quenched samples were tempered in conventional furnace at 300 °C for 1 h, corresponding to reference sample (untreated) (the sample hardness after tempering was 489±10 $HV_{0.3}$).

2.2 Low-temperature plasma carburizing treatment

Carburizing treatments were carried out in a conventional plasma apparatus (composed by a 4.16 kHz square-wave pulsed dc power supply), which is illustrated and described in detail on Scheuer *et al.* (2013). Samples were placed on the cathode of this system, which was negatively biased at 700 V. The heating of the samples was a result of ions and fast neutral species bombardment. The mean power transferred to the plasma, and consequently the sample temperature, was adjusted by varying the switched-on time (t_{ON}) of the pulsed voltage. The temperature was measured by means of a chromel–alumel thermocouple (Ktype of 1.5 mm diameter) inserted 8 mm depth into the sample holder. Initially, the vacuum chamber was evacuated to a base pressure of 1.33 Pa with the help a dual-stage mechanical rotary pump. Prior to carburizing treatments, specimens were plasma sputter-cleaned in a gas mixture of 80% H_2+20% Ar, under a pressure of 400 Pa, at 300 °C for 0.5 h, aiming to remove the native surface oxide layer. Plasma carburizing was carried out using a gas mixture composition of 99.5% (80% H_2+20% Ar)+0.5% CH_4, in volume. The total gas flow rate and pressure were fixed at 1.67×10^{-6} $Nm^3\ s^{-1}$ and 400 Pa, respectively. Both the gas mixture composition and flow rate were fixed according to Scheuer *et al.* (2012[b]), and the pressure and applied voltage in accordance with Scheuer *et al.* (2016). Samples were carburized at a fixed temperatures of 400 °C for times of 12, 24, 36 and 48 h; and 450 °C for times of 4, 8, 12 and 16 h. After carburizing, treated samples were cooled to room temperature under continuous flow of Ar and H_2 gas mixture (volume ratio: 1/4).

2.3 Surface and microstructural analysis

For microstructural analysis, samples were prepared by conventional metallographic procedure. After polishing, the cross-sectioned samples were etched using Marble's reagent (4 g of Cu_4SO_4 + 20 ml de HCl + 20 ml de H_2O). Samples were examined using an Optical Microscope (Olympus BX51M), and the thickness of the observed outer layers was determined by taking the mean of ten measurements using obtained images. The identification of the phases present in the treated layers was carried out by X-ray diffractometry (XRD), using a Shimadzu XRD 7000 X-ray diffractometer with a Cu Kα X-ray tube in the Bragg–Brentano configuration. The diffraction lines were taken with 2θ in the range of 30–60° with a scan speed of 0.1 θ/min. Surface roughness was measured using a Confocal Laser Scanning Microscope (Olympus LEXT OLS 3000). The measurements were made in a square area with 650 μm side, using a 20*x* objective lens, Gaussian filter and cut-off of 0.8 mm.

2.4 Electrochemical corrosion test

Electrochemical corrosion behavior of untreated and carburized AISI 420 steel samples were studied using potentiodynamic polarization technique. Cyclic potentiodynamic polarization curves were recorded according to the ASTM G61 standard, which is recommended for evaluating the pitting corrosion tendency of materials in chloride-containing media. The set up consisted of an Iviun Potentiostat/Galvanostat Model Iviun–n–Stat interfaced to a personal computer using the IviumSoft software, for data acquisition and analysis (using these software, the potentiodynamic polarization curves were plotted and both the corrosion current density (i_{cor}) and the zero current potential (E_{cor}) were

estimated), and an electrochemical corrosion cell. Experiments were carried out at ambient temperature (25 °C ± 2) and open to the air, using a graphite rod as counter electrode (CE) and saturated calomel electrode (SCE) as a reference electrode, and the specimen (AISI 420 steel disc) as the working electrode. Prior to each experiment, the electrodes surface were degreased with acetone, rinsed with deionized water, and dried in flow of heated air. The electrolyte used was 3.5 wt. % NaCl (*pH* = 6.9), obtained from the high-purity NaCl (99%), mixed with distilled water. The specimen was clamped to the cell, sealing against a silicone gasket, which exposes 50.24 mm^2 of the specimen surface to the electrolyte. After stabilizing the open circuit potential (OCP) for 60 min, cyclic polarisation measurement was performed potentiodynamically at a scan rate of 1 mV s^{-1}, by setting a potential value of 100 mV below the OCP, in the positive direction until a threshold current density of 5.0 $mAcm^{-2}$ was reached. At this point, the potentiodynamic scan was reversed to the negative direction, and continued down to starting point. Each experiment was repeated at least three times to check the reproducibility and the scatter in the data are reported. The specimen area exposed to the corrosive solution was subsequently analyzed with optical microscopy, used the same microscope described above.

3. RESULTS AND DISCUSSION

3.1 Microstructural characterization

Figure 1 depicts the cross section micrographs of samples carburized at 400 °C for (a) 12, (b) 24, (c) 36, and (d) 48 h. Results indicate the occurrence of a thin and continuous layer on the treated surface, which is constituted of Fe_3C and α'_C for samples carburized at 12 to 36 h, as indicated previously in the XRD data (Figure 2). For 48 h treatment condition, it appears the occurrence of sensitization along the outer layer, indicating the Cr carbides precipitation occurrence, already demonstrated by the XRD patterns. It can be also confirmed on Figure 1 (d) the occurrence of a diffusion layer below the outer layer for sample treated at 48 h, which is revealed by greater metallographic chemical etching intensity. In contrast, the diffusion layer for samples carburized between 12 to 36 h is only evidenced by profile hardness measurements, which are not presented here. According to Table 1, the outer and diffusion layer thickness increases with carburizing time, which indicates that the carbon transport into the steel surface is diffusion controlled, and the diffusion depth is proportional to the square root of time.

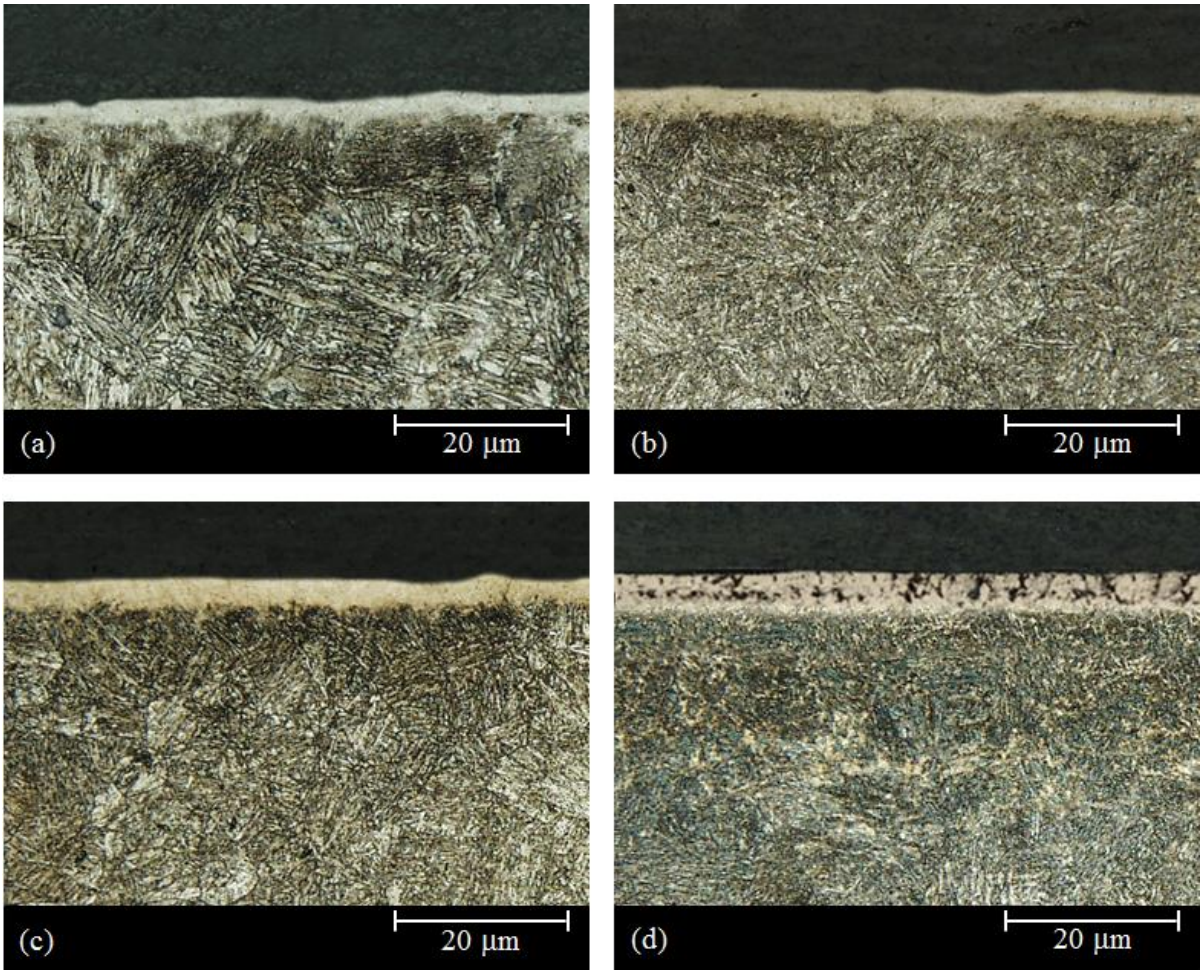

Figure 1. Cross-section micrographs of samples treated at 400 C for: (a) 12; (b) 24; (c) 36; and (d) 48h.

Table 1. Outer and diffusion layer thickness for samples carburized at 400 °C for 12, 24, 36 and 48 h, and for 450 °C for 4, 8, 12 and 16 h.

Treatment condition	400 °C		'Treatment condition	450 °C	
	Outer layer	Diffusion layer		Outer layer	Diffusion layer
12 h	2,3±0,16 μm	50 μm	4 h	1.5±0.1 μm	40 μm
24 h	3,0±0,24 μm	65 μm	8 h	2.2±0.2 μm	55 μm
36 h	3,8±0,17 μm	80 μm	12 h	2.7±0.2 μm	70 μm
48 h	4,4±0,23 μm	85 μm	16 h	3.0±0.2 μm	85 μm

As shown previously in another publication Scheuer *et al.* (2013) for samples carburized at 450 °C for 4 to 12 h, precipitation free layers are formed (composed by α'_C and Fe_3C). However, although there is no evidence of chromium carbides precipitation occurrence for samples treated at 16 h, it is believed that it has occurred in its initial stage since no clear precipitation is observed in the micrograph, and no Cr carbides peak reflections was observed on the XRD pattern.

Figure 2 shows the X-ray diffraction patterns of untreated and plasma-carburized samples treated at 400 °C for 12, 24, 36 and 48 h. For the 12–36 h treatment condition, it can be verified the formation of α'_C and Fe_3C phase. Furthermore, the 48 h carburizing condition shows the precipitation of Cr_7C_3 and $Cr_{23}C_6$ phases (which is confirmed by the sensitization observed in Figure 1d), and the α'_C to α–Fe phase decomposition as a result of the intense chromium carbides precipitation.

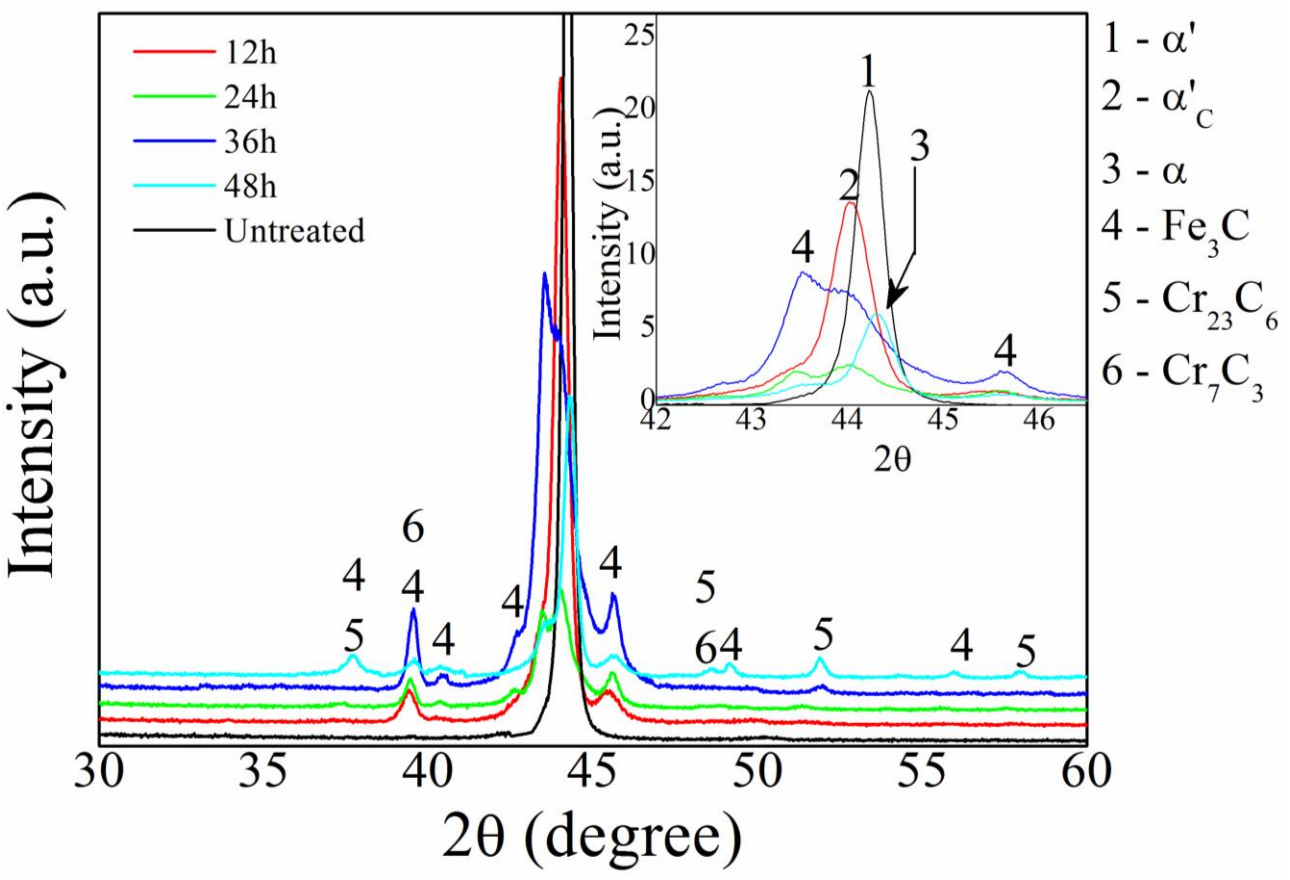

Figure 2. XRD patterns for untreated sample and for samples treated at 400 °C for 12, 24, 36 and 48 h.

3.2 Corrosion behavior

In order to improve understanding of treatment parameters influence on the corrosion behavior of carburized AISI 420 steel, the treatment temperature was set at 400 and 450°C and the effect of treatment time was evaluated in the range of

4 to 48h. Corrosion behavior was found to be depend on microstructural changes promoted by the carburized time variation. Thereby, Figure 3 (a) present the open circuit potential test results for samples carburized at 400 °C for 12, 24, 36 and 48 h, as well for the reference condition. It appears the same behavior verified on previously shown results (temperature cycle): the initial decrease of OCP to less noble values with subsequent stabilization, which implying that a stable film/solution interface was produced. Furthermore, is noticed a reduction on OPC-values with treatment time rise (seen also Table 2), and only the 48 h condition presented a E_{OC} below to the untreated samples, signaling the reduced corrosion resistance of samples carburized at this condition (fomented by Cr carbide phase formation – Figure 1 and Figure 2). Although employed microstructural characterization techniques have not shown the chromium carbide precipitation occurrence for samples carburized at 24 and 36 h, one cannot rule out the formation of chromium carbides nanosized precipitates, which would justify the corrosion resistance deflection when compared to 12 h. Cyclic polarization curves (Figure 3b) indicate the maintenance of the same behavior of OCP test results: decrease of the corrosion potential to more negative values (less nobler) with increasing treatment time (Table 2). As can be seen from Figure 3 (b), only sample carburized for 24 h present a passivation region, however the passivation did not promote an improvement in corrosion behavior. It is also noticed that potentiodynamic curves of untreated and 36-48 h carburized samples are displaced upward (for higher current density values), that supports the assumption of decreasing on corrosion resistance with the increase on processing time. Finally, potentiodynamic curves no indicate the occurrence of repassivation phenomenon being that the hysteresis positive loop indicates the passive layer breakdown with pitting corrosion occurrence.

Table 2. Electrochemical parameters obtained from the corrosion tests for samples treated 400 °C for 12, 24, 36 ando 48 h, and for 450 °C for 4, 8, 12 and 16 h.

Treatment condition		Electrochemical parameters				
Temperature	Time	E_{OC} (V *x* NHE)	E_{COR} (V x NHE)	E_{PIT} (V x NHE)	i_{CORR} (mA/cm^2)	TC (mm/year)
400 °C	12 h	-0,1751	-0,1764	–	1,96	0,022
	24 h	0,0442	0,0427	–	1,09	0,012
	36 h	-0,05154	-0,0283	0,3233	1,41	0,016
	48 h	-0,13478	-0,1211	–	1,34	0,015
450 °C	4 h	-0,1751	-0,1764	–	1,96	0,022
	8 h	-0,13478	-0,0676	–	1,08	0,012
	12 h	0,00845	0,0427	–	0,94	0,010
	16 h	-0,0587	-0,0142	0,1634	1,12	0,012
Untreated (reference)		-0,1751	-0,1764	–	1,96	0,022460073

The OPC values after potential stabilization for higher temperatures treatments (450 °C) but for lowest carburizing times (4 to 16 h) (Figure 4a), are similar than shown above in Figure 3(a) for samples treated at 400 °C for long treatment times (12 to 48 h). OCP values for increased treatment time up to 8 h stabilized at a growing nobler potential values (more positive). Sample treated for 12 h showed a decreasing E_{OC}, but still nobler than the untreated and 4 h treatment condition. The 16 h treatment condition moreover, is the only studied condition that presents less noble potential confronted with untreated sample. Again, it is believed that the occurrence of nanosized precipitates are responsible for the decrease on OCP potential from 8 to 12 h at 450 °C. Therefore, additional microstructural characterization, are required to prove this hypothesis. Nanosized coherent precipitates occurrence on H13 tool steel after plasma nitriding was observed by Zagonel *et al.* (2012) using the High-Resolution Transmission Electron Microscopy (HR-TEM). Therefore, further studies using HR-TEM technique well be performed to confirm this assumption. Figure 4 (b) show the polarization curves of samples treated at 450 °C for 4 to 16 h, from which can be observed that E_{COR} values follows the same behavior of E_{OP}. Moreover, it is noted that as observed for the previously analyzed conditions, the hysteresis positive loop indicates the protective layer collapse with pitting corrosion occurrence, and the curves do not indicate the passivation occurrence. Ultimately, it is noted that the potentiodynamic curves for samples treated in times below 12 h are shifted to lower current densities, confirming its best corrosion resistance on studied medium when compared to untreated and 16 h carburized samples.

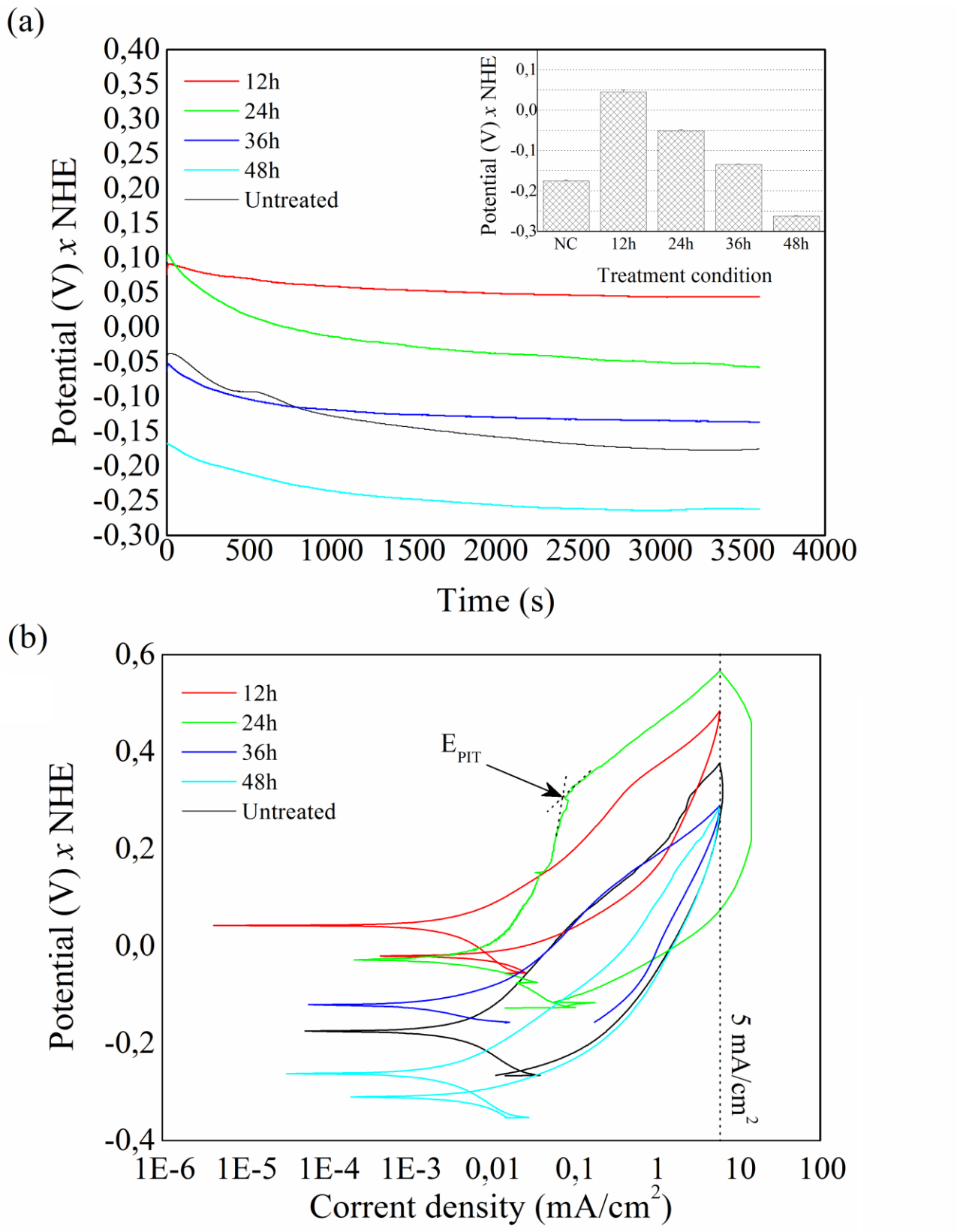

Figure 3. (a) Open circuit potential, and (b) potentiodynamic polarization curves achieved in a 3.5% NaCl solution of untreated and AISI 420 steel samples plasma carburized at 400 °C for 12, 24, 36 and 48 h.

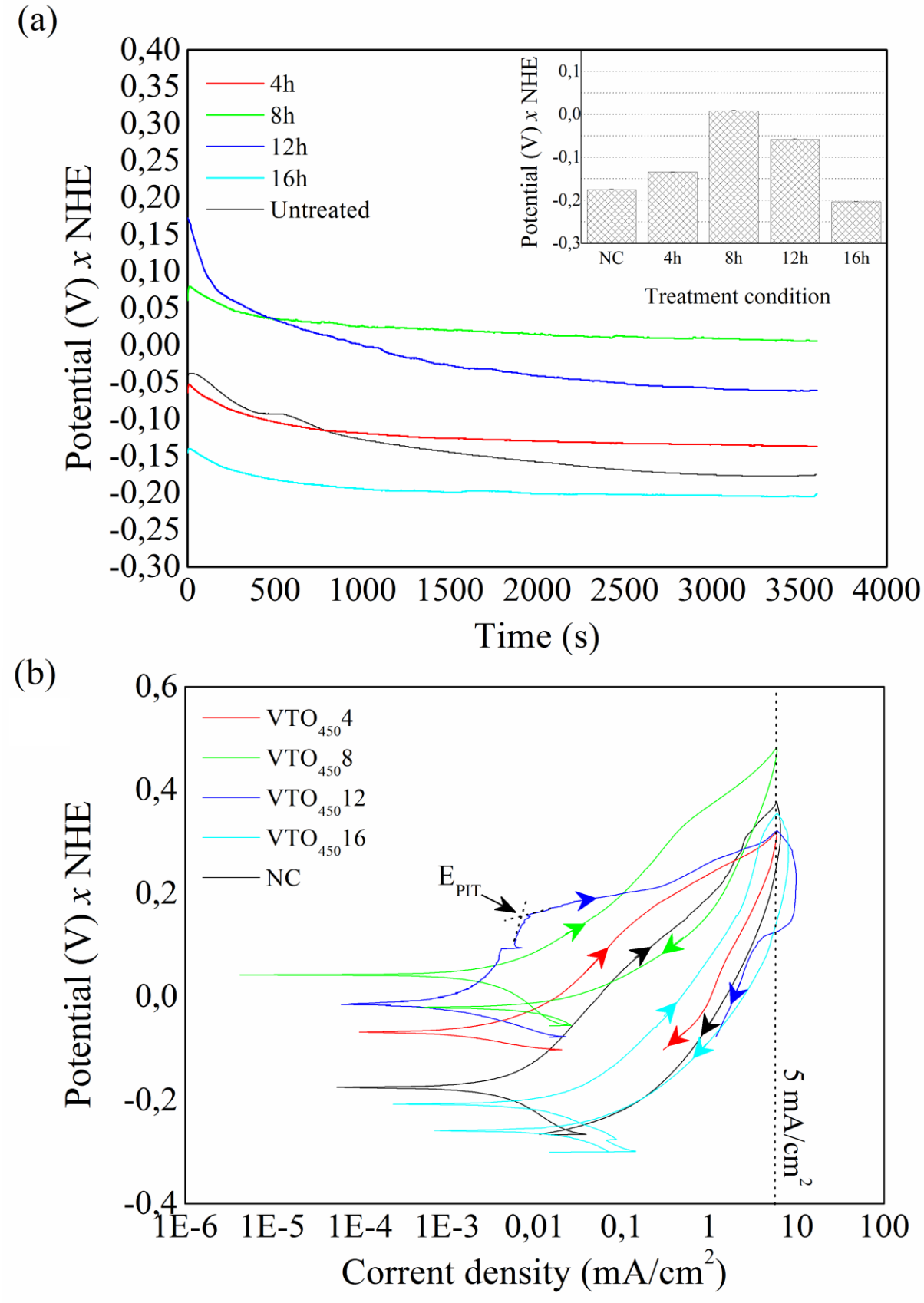

Figure 4. (a) Open circuit potential, and (b) potentiodynamic polarization curves achieved in a 3.5% NaCl solution of untreated and AISI 420 steel samples plasma carburized for 450 °C for 4, 8, 12 and 16 h.

Morphological analysis (Figure 5 and Figure 6) performed on samples after the cyclic polarization test shows a pattern which is in agreement with the results previous presented for 400 (Figure 3) and 450 °C (Figure 4) treated samples, respectively. There is an increase in the pits density with the addition of treatment time from 12 to 48 h (Figure 5),

confirming the decreasing of corrosion resistance with treatment time increasing. In these cases, possibly the existence of defects along the outer layer, such as secondary phases precipitates (and consequent impoverishment located of Cr), and their increased occurrence with the increase on processing time, is the cause of most intense corrosive attack Pardo *et al*. (2008). On Figure 6, there is the reduction in the pits density from 4 to 12 h, with subsequent addition to 16 h condition. Latter condition has suffered a more intense corrosion attack, confirming their lowest corrosion resistance. Finally, is noted that apparently the pits of the sample treated for 8h present shallower, confirming its better corrosion behavior already indicated.

Regarding the electrolytic solution characteristics used in polarization tests of samples from time variation cycle, after the tests there was no a marked change in the pH of the substance when compared to that measured prior to the electrochemical tests. Finally, it was not detected the presence of solid precipitates on solution after tests, indicating that for presented processing conditions the corrosion resistance is better that those observed for samples treated at 500 °C for 8 and 12 h showed in part I of this study.

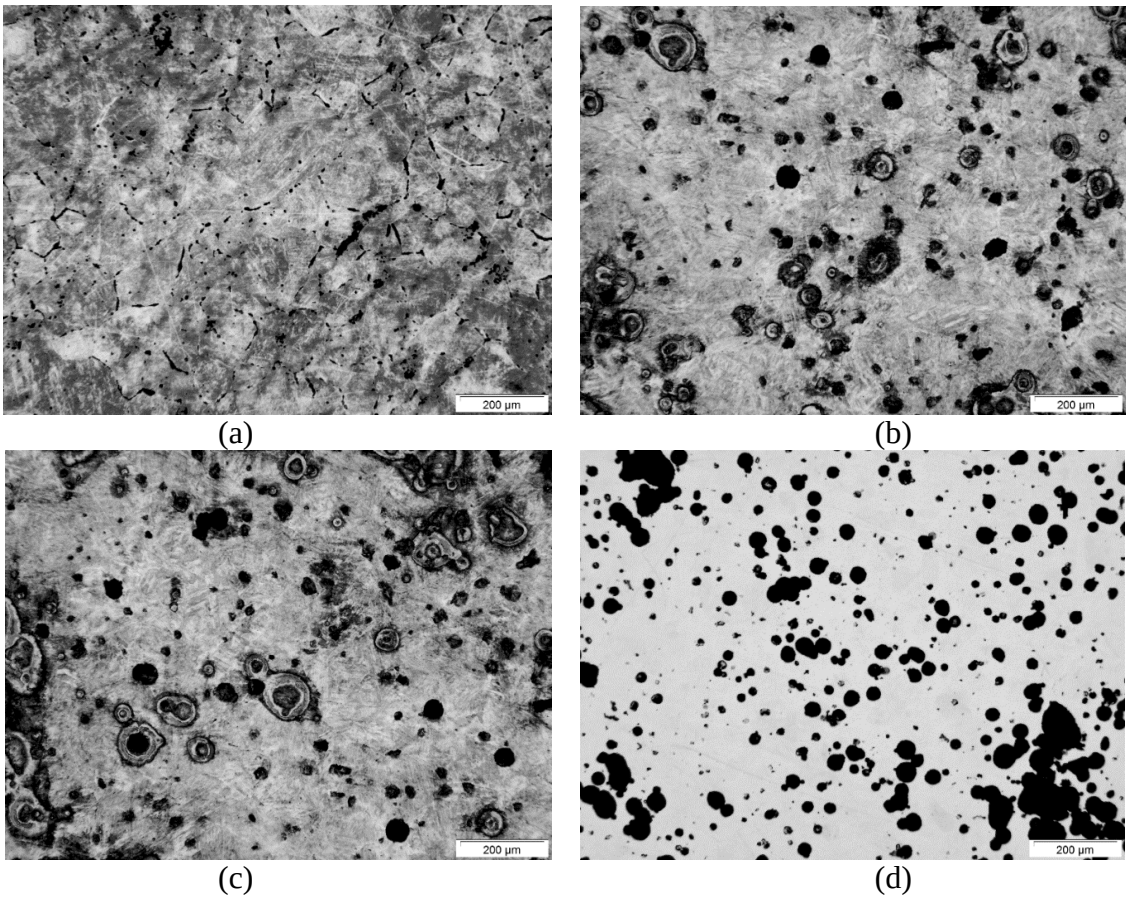

(a) (b)

(c) (d)

Figure 5. Optical microscopy morphologies of samples plasma carburized at 400 °C (a) 12, (b) 24, (c) 36 and (d) 48 h after corrosive test.

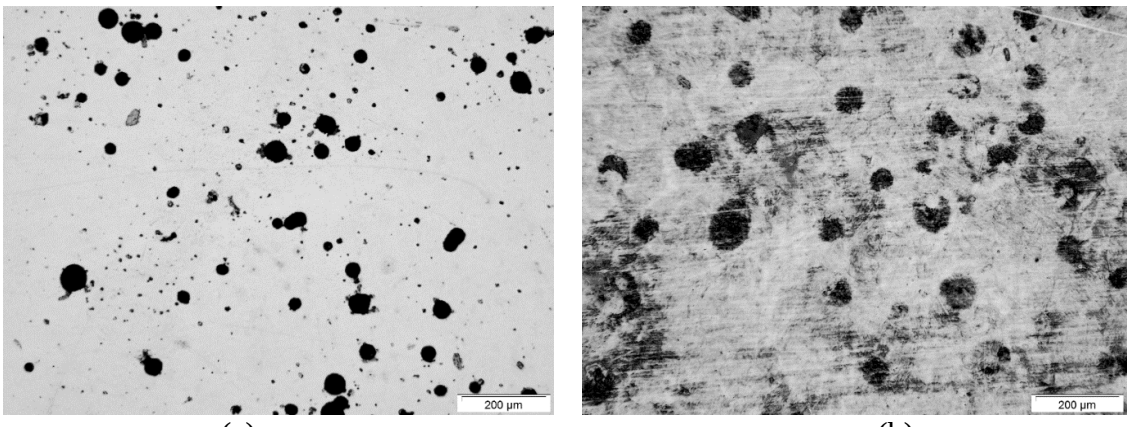

(a) (b)

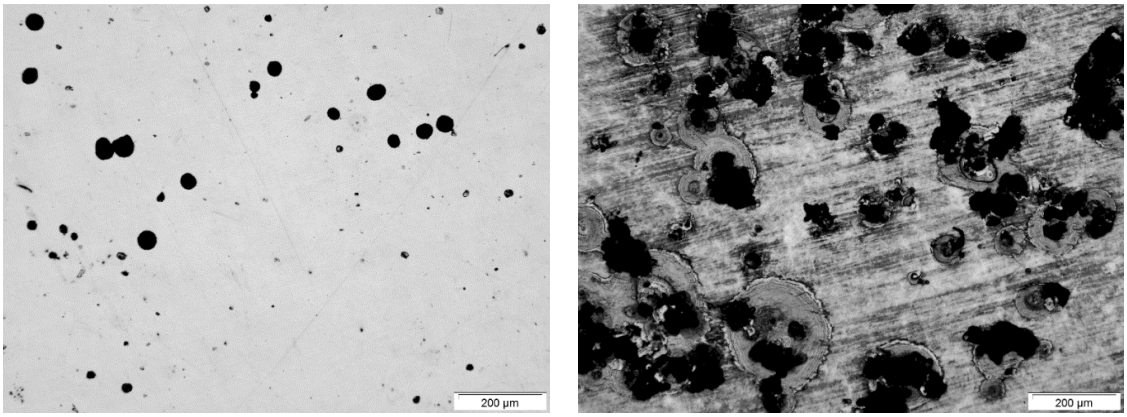

(c) (d)

Figure 6. Optical microscopy morphologies of samples plasma carburized at 450 °C (a) 4, (b) 8, (c) 12 and (d) 16 h after corrosive test.

4. CONCLUSION

- Microstructural characterization revealed that carburized layer is formed through two distinct regions: an outer layer composed by Fe_3C and α'_C; and a diffusion layer, which is composed only by α'_C phase. It was also shown that the thickness of these two layers increases with increasing carburising temperature;
- Plasma carburized samples have a more noble corrosion behavior when compared to the reference sample (untreated), with the exception of those carburized at prolonged times (48 h for 400 ° C and 16 h for 450 °C). The improvement in the electrochemical behavior is due to the formation of a hardened layer ($Fe_3C + \alpha'_C$). The decrease in corrosion resistance for samples carburized at high temperature, is credited to the occurrence of chromium carbide phases precipitation, causing sensitization;
- The corrosion mechanism of carburized samples is the pitting corrosion.

5. REFERENCES

C.A. Figueroa, F. Alvarez, Z. Zhang, G.A. Collins, K.T. Short. Journal Of Vacuum Science & Technology A 23 (2005) 693 – 698.

C.J. Scheuer, R.P. Cardoso, R. Pereira, M. Mafra, S.F. Brunatto. Materials Science And Engineering: A 539 (2012) 369–372.

C.J. Scheuer, R.P. Cardoso, F.I. Zanetti, T. Amaral, S.F. Brunatto. Surface & Coatings Technology 206 (2012) 5085–5090.

C.J. Scheuer, R.P. Cardoso, M. Mafra, S.F. Brunatto. Surface & Coatings Technology 214 (2013) 30–37.

C.J. Scheuer, R.P. Cardoso, M. Mafra, S.F. Brunatto. *Submitted In Plasma Processes And Polymers.*

C.X. Xi, D.X. Liu, D. Han. Acta Metallurgica Sinica (English Letters) 21 (2008) 21–29.

C.X. Li, T. Bell. Corrosion Science 48 (2006) 2036–2049.

C.X. Li, T. Bell. Materials Science And Technology 23 (2007) 355–361.

E.A. Bernardelli, P.C. Borges, L.C. Fontana J.B. Floriano. Kovové Materiály, 48 (2010) 105–116.

E. Leitao, R.A. Silva, M.A. Barbosa. Corrosion Science 44 (2002) 2393–2407.

F.J. Martin, E.J. Lemieux, T.M. Newbauer, R.A. Bayles, P.M. Natishan, H. Kahn, G.M. Michal, F. Ernst, A.H. Heuer, Electrochemical And Solid-State Letters 10 (2007) C76-C78.

G.H. Aydoğdu, M.K. Aydinol. Corrosion Science 48 (2006) 3565–3583.

I. Alphonsa, A. Chainani, P.M. Raole, B. Ganguli, P.I. John. Surface And Coatings Technology 150 (2002) 263–268.

I. Taji, M.H. Moayed, M. Mirjalili. Corrosion Science 92 (2015) 301–308.

J. Flis, M.K. Wydorska, I.F. Kabulska. Journal Of Solid State Electrochemistry 10 (2006) 689–695.

J. Flis, M.K. Wydorska. Journal Of The Electrochemical Society 151 (2004) B573–B580.

J.M. Aquino, C.A. Della Rovere, S.E. Kuri. Corrosion Science 51 (2009) 2316–2323

L.F. Zagonel, J. Bettini, J.; R.L.O Basso Et Al. Surface And Coatings Technology, 207 (2012) 72–78.

M.C. Pardo, A.E. Merino, F. Coy, R. Viejo, E. Arrabal, E. Matykina.. Corrosion Science 50 (2008) 1796–1806

M.K. Wydorska, J. Flis. Corrosion Science 50 (2008) 523–533.

N. Alonso-Falleiros, M. Magri, I.G.S. Falleiros Corrosion 55 (1999) 769–778.

P. Corengia, G. Ybarra, C. Moina, A. Cabo, E. Broitman. Surface And Coatings Technology 187 (2004) 63–69.

P. Corengia, F. Walther, G. Ybarra, S. Sommadossi, R. Corbari, E. Broitman. Wear 260 (2006) 479–485.

R.R.M. De Sousa, F.O. De Araújo, K.J.B Ribeiro, T. Dumelow, J.A.P. Da Costa, C. Alves Jr. Surface And Coatings Technology 24 (2008) 52–56.

S. Frangini, A. Mignone. Corrosion 48 (1992) 715–726.

S.K. Kim, J.S. Yoo, J.M. Priest, M.P. Fewell. Surface And Coatings Technology 163-164 (2003) 380–385.

S. P. Brühl, R. Charadia, S. Simison, D.G. Lamas, A. Cabo. Surface & Coatings Technology 204 (2010) 3280–3286.

S.S.M. Tavares, F.J. Da Silva, C. Scandian, G.F. Da Silva, H.F.G. De Abreu. Corrosion Science 52 (2010) 3835–3839.

S.Y. Lu, K.F. Yao, Y.B. Chen, M.H. Wang, N. Chen, X.Y. Ge. Corrsaion Science, *In Press* (2015).

V. Kain, K. Chandra, K.N. Adhe, P.K. De. Corrosion 61 (2005) 587–593.

V.V. Nikam, R.G. Reddy, S. Collins, P.C. Williams, G.H. Schiroky, G.W. Henrich. Electrochimica Acta 53 (2008) 2743-2750.

X.Y. Li, S. Thaiwatthana, H. Dong, T. Bell. Surface Engineering 18 (2002) 448–452.

Y. Xi, D. Liu D.; D. Han. Surface And Coatings Technology 202 (2008) 2577–2583.

Y. Xi, D. Liu, D. Han. Applied Surface Science 254 (2008) 5953–5958.

Y. Sun, T. Bell, G. Wood. Wear. 178 (1994) 131–138.

Y. Sun. Journal Of Materials Processing Technology. 168 (2005) 189–194.

6. RESPONSIBILITY NOTICE

The authors are the only responsibles for the content of this work.